Journal of
Materials in Life Sciences

Vol. 3 No. 2 (2024)

Full Paper

Green Synthesis of Magnesium Oxide Nanoparticles using *Asystasia gangetica* and its Antibacterial Study Against Gram-Positive and Gram-Negative Bacteria

Nur Aida Fatimah Mashri[a,b], Muhammad Amir Akhtar Mohd Azizul[a], Hanis Mohd Yusoff[a,c,*], Nurhanna Badar[a,c], Siti Nor Khadijah Addis[a], Nik Ahmad Nizam Nik Malek[d,e]

[a] Faculty of Science and Marine Environment, Universiti Malaysia Terengganu, 21030 Kuala Nerus, Terengganu, Malaysia.
[b] Department of Chemical Sciences, Faculty of Science and Technology, Universiti Kebangsaan Malaysia, 43600 Bangi, Selangor, Malaysia.
[c] Advanced Nano Materials (AnoMa) Research Group, Faculty of Science and Marine Environment, Universiti Malaysia Terengganu, 21030 Kuala Nerus, Terengganu, Malaysia.
[d] Department of Biosciences, Faculty of Science, Universiti Teknologi Malaysia, 81310 UTM Johor Bahru, Johor, Malaysia.
[e] Centre for Sustainable Nanomaterials, Universiti Teknologi Malaysia, 81310 UTM Johor Bahru, Johor, Malaysia.

Article history
Received
26 November 2024
Revised
3 December 2024
Accepted
6 December 2024
Published online
8 December 2024

*Corresponding author
hanismy@umt.edu.my

Abstract

Magnesium oxide nanoparticles (MgO-NPs) have various potential in medicine, catalysis and electronics due to their tailored properties on side and shape. It is important to obtain MgO-NPs by using green synthesis approach through the utilization of various parts of plants, such as the aloe vera plant, rambutan seeds, and clove flower, in synthesizing MgO-NPs. In this study, MgO-NPs are produced using *Asystasia gangetica* plant extract via the green combustion method. Characterization involves Thermal Gravimetric Analysis (TGA), Fourier Transform Infrared Spectroscopy (FTIR), X-ray Diffraction (XRD), Scanning Electron Microscopy (SEM), UV-Vis Spectroscopy (UV-Vis), and Accelerated Surface Area and Porosimetry (ASAP). TGA results reveal that MgO achieves its stability around 650 °C, leading to the determination of the calcination temperatures at 700 °C and 800 °C. FTIR analysis reveals Mg-O stretching (670 cm^{-1} to 700 cm^{-1}). XRD and SEM show high crystalline MgO-NPs with particle sizes of about 149 - 298 nm. ASAP indicates mesoporous characteristics with plate-like pores. Antibacterial activities were evaluated through a well diffusion method using Gram-positive (*Staphylococcus aureus*) and Gram-negative (*Escherichia coli*) bacteria. Antibacterial activity against *Staphylococcus aureus* is significant at concentrations of 500 mg/mL for MgO-NPs calcined at 800 °C, while no significant activity is observed against *Escherichia coli.* The promising results of green synthesis have high potential for further study.

Keywords MgO-NPs, green synthesis, nanoparticles, antibacterial activity

1.0 INTRODUCTION

Nanomaterials have already been notable for particular characteristics of high reactivity, strength, and conductivity. Magnesium oxide nanoparticles (MgO-NPs) are known to be versatile with strong characteristics. Its applications range from medicine

through catalysis to electronics [1-3]. On the other hand, there are some serious risks to environmental and human health because conventional nanoparticle synthesis usually employs hazardous chemical substances, demanding high-energy input. Green synthesis was developed as an environmentally friendly alternative, using various natural materials in the form of plant extracts to reduce and stabilize nanoparticles with minimal harm towards environmental and without resorting to harmful chemicals [4-6]. This study highlights the utilization of plant extracts dealing with green syntheses route for nanoparticle synthesis. One of the challenges in green synthesis is finding plants with abundant resources, maturity and appropriate harvest times. Hence it is important to find non seasonal plants that are easily available and possess additional medicinal properties for applications in antibacterial studies [2-4].

Asystasia gangetica is a medicinal plant known for its antimicrobial action and hence forms a very excellent bioresource for the green synthesis approach. The reduction of metal ions by the bioactive compounds such as alkaloids, flavonoids, and phenols present in this plant helps in stabilizing the nanoparticles specifically in obtaining silver nanoparticles (AgNPs) [7]. The plant has not been utilized in the green synthesis of metal oxide nanoparticles hence is considered an ideal candidate for the eco-friendly production of MgO-NPs. A study on the green synthesis of MgO-NPs using the extract of *Asystasia gangetica* with characterization of its physicochemical properties and testing its antibacterial activity was conducted. Attention is given to their efficacy against resistant pathogens such as *Escherichia coli* and *Staphylococcus aureus*. In this respect, the present work falls within the frame of an increasing number of studies dealing with biosustainable nanotechnology because the method used was green synthesis from plants and could indicate the possibility of considering MgO-NPs as efficient and eco-friendly antibacterial compounds. The findings in this present study may open up a source for developing new biomaterials that are biocompatible, inexpensive, and suitable for various biomedical and industrial applications.

2.0 EXPERIMENTAL

2.1 Materials

Magnesium nitrate hexahydrate ($Mg(NO_3)_2{\cdot}6H_2O$) were purchased from Sigma Aldrich and served as the primary chemical for synthesizing MgO-NPs. Whatman No 1 filter paper was used for filtering, and distilled water was utilized in all aqueous solutions. Reagents for phytochemical analysis, including iodine solution (I_2), potassium iodide (KI), concentrated sulphuric acid (H_2SO_4), hydrochloric acid (HCl), acetic anhydride ($(CH_3CO)_2O$), iron (III) chloride ($FeCl_3$), β-naphthol and ethanol were all purchased from Sigma Aldrich.

2.2 Preparation of *Asystasia gangetica* Leaves Extract

Asystasia gangetica plants were collected from residential areas and roadsides in the Kuala Nerus district. The plants were thoroughly washed under running tap water, followed by rinsing with Milli-Q deionized water [4-6]. Next, they were dried in oven at 100 °C for 4 hours to remove moisture and prevent clogging during grinding, resulting in fine powders. Two grams of dried plant powder was mixed with 100 mL of Milli-Q water and heated in a water bath at 100 °C while being continuously stirred for 15 minutes. The crude extract was then filtered using Whatman No. 1 filter paper. The filtrate was collected and used for the green synthesis of MgO-NPs.

2.3 Green Synthesis of Magnesium Oxide Nanoparticles (MgO-NPs)

Magnesium oxide nanoparticles (MgO-NPs) were synthesized via a green combustion method [4-6]. The process began by mixing 5 mL of *Asystasia gangetica* plant extract, 5 mL of deionized water with 1 M solution of magnesium nitrate hexahydrate. The solution was stirred continuously for 15–20 minutes to attain homogeneity. The homogeneous solution obtained was transferred into a crucible and then heated in the preheated furnace at 500 °C for 15 minutes to form the MgO precursors. This precursor was further calcined at two specific temperatures, as determined by the TGA analysis, to finally produce the MgO-NPs.

2.4 Characterization of Materials

TGA of MgO precursors was carried out to investigate the calcination temperature. About 10 mg of the precursor was considered for thermal characterization using a Mettler Toledo TGA instrument, providing both weight loss and Differential Thermal Analysis (DTA) curves.

The prepared MgO-NPs were characterized by various analytical techniques: Fourier Transform Infrared Spectroscopy, X-Ray Diffraction, Scanning Electron Microscopy, Ultraviolet-Visible Spectroscopy, and Accelerated Surface Area and Porosimetry. FTIR structural analysis was done using a Tescan Bruker FT-IR spectrometer with OMNIC software and the Attenuated Total Reflectance technique. About 5 mg of the sample was placed in the sample holder and the spectrum was recorded over the range of 4000–400 cm^{-1} [6-8]. Crystallinity and phase composition analysis of MgO-NPs was done on an X-

ray diffractometer (XRD-6000, Shimadzu, Japan) using Cu Kα radiation (λ = 0.15412 nm) over the scanning range of 20–80° at a rate of 0.05°/min and a time constant of 2 seconds. All samples were prepared by grinding in an agate mortar and pestle. Surface morphology was carried out using a Floor Top SEM, Tescan Bruker, which was operated at an accelerating voltage of 30 kV with a spatial resolution of 50–100 nm with magnification ranging from 5,000X to 30,000X. The optical properties of MgO-NPs were studied with the help of a Shimadzu UV-1800 spectrophotometer in the range of 250–800 nm at room temperature. In this work, one spatula of MgO-NPs was added to 80 mL of distilled water and stirred overnight to form a suspension. Further, in this study, surface area, pore size, and adsorption-desorption isotherm were evaluated on an ASAP 2020 Micromeritics instrument using nitrogen gas as the adsorbate [6-8]. These measurements described the porosity and textural characteristics of MgO-NPs in detail.

2.5 Antibacterial assay

2.5.1 Well Diffusion Method

The well diffusion technique was employed to study of the MgO-NPs antibacterial activities against *Staphylococcus aureus* (gram-positive) and *Escherichia coli* (gram-negative). For this purpose, subcultures were made from pure culture onto agar plates and similarly incubated for a period of 24 hours. Further, a bacterial suspension was prepared by diluting a colony in 0.9% NaCl solution and adjusting it to the 0.5 McFarland standard to ensure homogeneous bacterial growth. All bacterial strains were streaked on Muller Hinton agar plates using sterile cotton buds. Circular discs impregnated with nanoparticle suspensions were placed on the agar surface. The plates were then placed in an incubator at 37 °C for 24 hours, which allowed the MgO-NPs to interact with the bacterial culture. After incubation, the measurement of zones of inhibition (ZOI) around the discs was carried out to determine the antibacterial efficacy of the nanoparticles. Deionized water was used as the negative control, and gentamicin was used as the positive control to get a comparison versus a standard antibiotic [9-10].

3.0 RESULTS AND DISCUSSION

3.1 Phytochemical Study of *Asystasia gangetica* Leaves Extract

Phytochemical tests were conducted for the qualitative identification of active compounds from Asystasia gangetica responsible for reducing and stabilizing MgO-NPs. The plant extract was treated with Wagner's test, H_2SO_4 test, Foam test, Tannin test, and Phenolic content test in triplicates to confirm the presence of bioactive components. The results obtained are summarized in detail in Table 1.

Table 1 Phytochemicals tests results of *Asystasia gangetica*

Active compounds	Replicate 1	Replicate 2	Replicate 3
Alkaloid	+	+	+
Flavonoid	+	+	+
Carbohydrates	+	+	+
Steroid	+	+	+
Tannin	+	+	+
Phenolic group	+	+	+
Saponin	-	-	-

(+) indicate the presence of active compounds in the *Asystasia gangetica* plant
(-) indicate the absence of active compounds in the *Asystasia gangetica* plant

The presence of various bioactive principles like alkaloids, flavonoids, carbohydrate, steroids, tannins, and phenolic compounds has been reported in the extract of *Asystasia gangetica*, as shown by Table 1. The phenolic compounds and tannins present in this plant, due to the hydroxyl group, act as reducing and stabilizing agents, which may reduce the Mg^{2+} to Mg and usually stabilize MgO-NPs [11]. Furthermore, phenolic compounds show potential in antibacterial, anti-inflammatory, and antioxidant activities, proving to be effective against different species of bacteria. In fact, a study by [9] has also presented evidence that the antibacterial efficacy is due to these phenolic compounds.

3.2 Characterization of MgO and MgO-NPs

3.2.1 Thermogravimetric Analysis (TGA)

TGA analysis was employed to determine the thermal stability and calcination temperature required. Figure 1 indicates that the MgO precursor decomposed in two steps with 1.2% and 1.8% weight losses. The increase in temperature continued resulting in a weight loss, which stabilized at about 650 °C. Based on this observation, calcination temperatures of 700 °C and 800 °C were selected in accordance with [6-8, 12] to form the MgO-NPs. The precursor was then divided into two portions and calcined at each of the temperatures mentioned above for 8 hours.

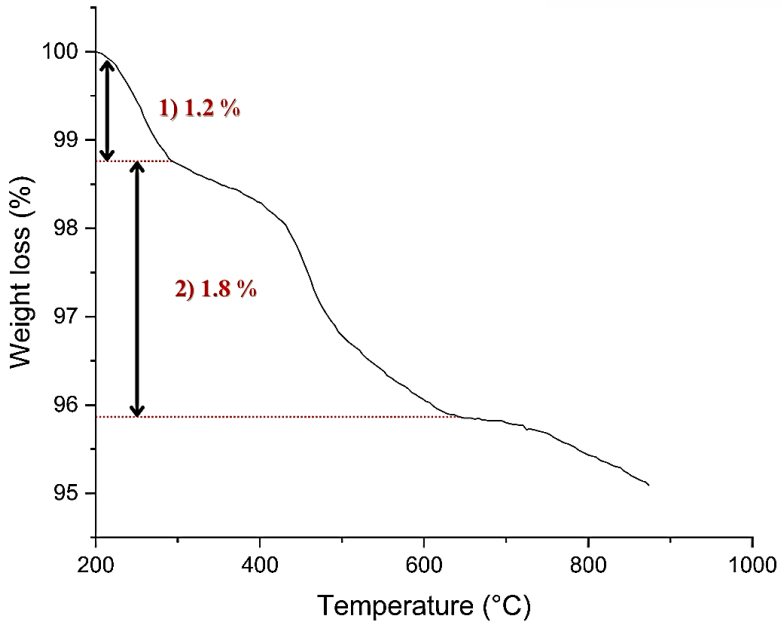

Figure 1 TGA thermogram of MgO precursor

3.2.2 Fourier Transform Infrared Spectroscopy (FT-IR)

The FT-IR was used to identify the chemical composition, functional groups, and molecular interactions of MgO-NPs. Figure 2 shows the FT-IR spectrum of *Asystasia gangetica* plant in powder form. Figure 3 presents comparative FT-IR spectra of MgO powder before calcination and MgO-NPs calcined at 700 °C and 800 °C.

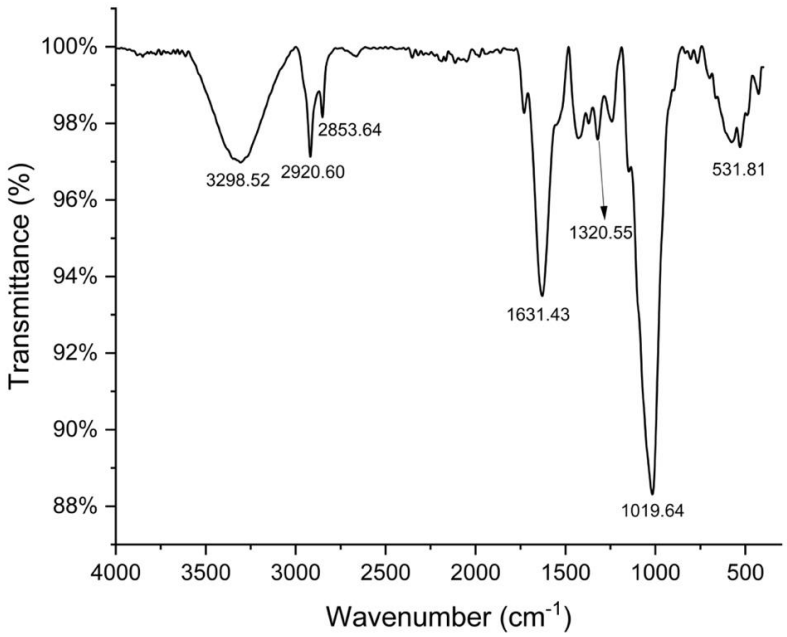

Figure 2 FT-IR spectrum of *Asystasia gangetica* plant in powder form

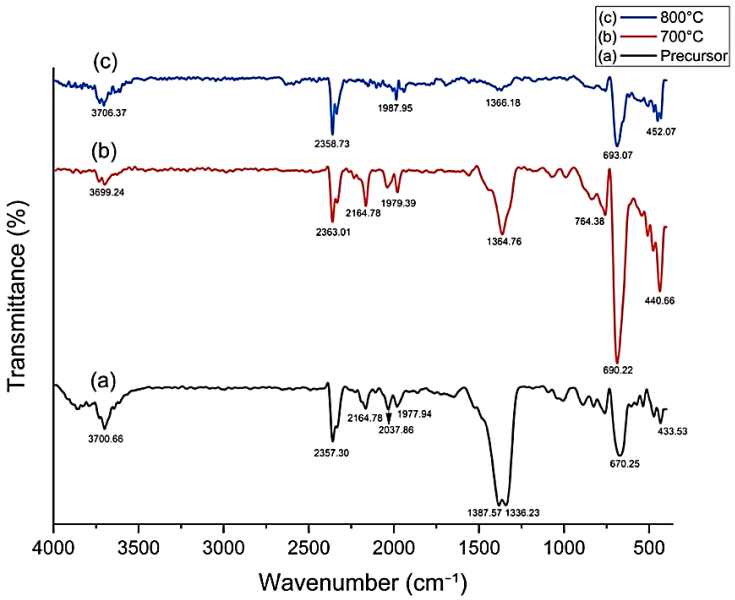

Figure 3 FT-IR spectra of MgO before and after the calcination process

The infrared spectrum of the powder of *Asystasia gangetica* is shown in Figure 2, revealing various functional groups. The broad band at 3298.52 cm^{-1} indicates O-H stretching vibrations, pointing to alcohols, phenols, or carboxylic acids. Peaks at 2920.60 cm^{-1} and 2853.64 cm^{-1} are assigned to C-H stretching vibrations, demonstrating alkanes, alkenes, or alkynes. The band at 1631.43 cm^{-1} is attributed to C=C stretching, relating to alkenes [16], while the band at 1320.55 cm^{-1} signifies C-N stretching, indicating amines or amides. The band at 1019.64 cm^{-1} indicates C-O stretching, which could be due to alcohols, ethers, or esters. Finally, the band at 531.81 cm^{-1} is attributed to C-C stretching, suggesting alkanes, alkenes, or alkynes [13].

Figure 3 depicts comparative FT-IR spectra of the non-calcined MgO powder (a), MgO-NPs calcined at 700 °C (b), and MgO-NPs calcined at 800 °C (c). All samples show an O-H stretching band in the broad range around 3700 cm^{-1}, with the precursor (a) having the largest intensity compared to the calcined samples (b and c), indicating that calcination led to the removal of water [14]. A weak N=C=O peak at 2358 cm^{-1} in (c) suggests residual organic matter, with stronger peaks in (a) and (b) [1]. The C≡C and C=O peaks observed at approximately 2164 cm^{-1} (a, b) and 1987 cm^{-1} (c), respectively, show organic residues. While highlighting organic material, the N-O stretching peaks at 1387 cm^{-1} (a), 1364 cm^{-1} (b), and 1366 cm^{-1} (c) also evidence organics in the samples studied here [6]. Sample (a) shows a band due to C-H stretching at 2037 cm^{-1}, which is absent in calcined samples, confirming the removal of organic groups by calcination. All the samples in the figure show a strong Mg-O bending band at 450 cm^{-1}, which shifted to higher wavenumber positions in samples (b) and (c), indicating stronger Mg-O bonds after calcination. These stretching peaks at 670 cm^{-1} (a), 690 cm^{-1} (b), and 693 cm^{-1} (c) confirm the formation of MgO-NPs [1]. Band assignments are summarized in Table 2.

Table 2 Band assignment of FT-IR spectra

Band assignment	**Wavenumber (cm^{-})**		
	MgO precursor (a)	MgO calcined at 700 °C (b)	MgO calcined at 800 °C (a)
O-H stretching	3700.66	3699.24	3706.37
N=C=O stretching	2357.30	2363.01	2358.73
C≡C stretching	2164.78	2164.78	-
C-H stretching	2037.86	-	-
C=O stretching	1977.94	1979.39	1987.95
N-O stretching	1387.57	1364.76	1366.18
	1336.23		
Mg-O stretching	670.25	690.22	693.07
Mg-O bending	433.53	440.66	452.07

3.2.2 X-Ray Diffraction (XRD)

XRD analysis was utilized to evaluate the composition and quality of substances. Figure 4 presents XRD diffractograms for commercial MgO and for MgO-NPs calcined at 700 °C and 800 °C. All the samples exhibit sharp peaks, indicating high crystallinity with a cubic crystal structure. The diffraction peaks at 36.8°, 42.8°, 62.1°, 74.5°, and 78.4° correspond to the (111), (200), (220), (311), and (222) planes of MgO, respectively. These peaks align with the JCPDS card No. 87-0653, confirming the polycrystalline cubic structure [10].

The sharp peaks observed for MgO-NPs calcined at 800 °C indicate well-formed MgO crystals with larger sizes. On the other hand, the commercial MgO (a) shows slight peak splitting at 36.85°, potentially due to traces of $Mg(OH)_2$ [6]. The broader peaks in the MgO-NPs calcined at 700 °C (b) suggest smaller and less well-formed crystals compared to those calcined at 800 °C. These findings are consistent with previous research, such as the study by [6], which reported similar results using *Mariposa christia vespertilionis* leaf extract. The XRD data for both commercial and synthesized MgO are summarized in Table 3.

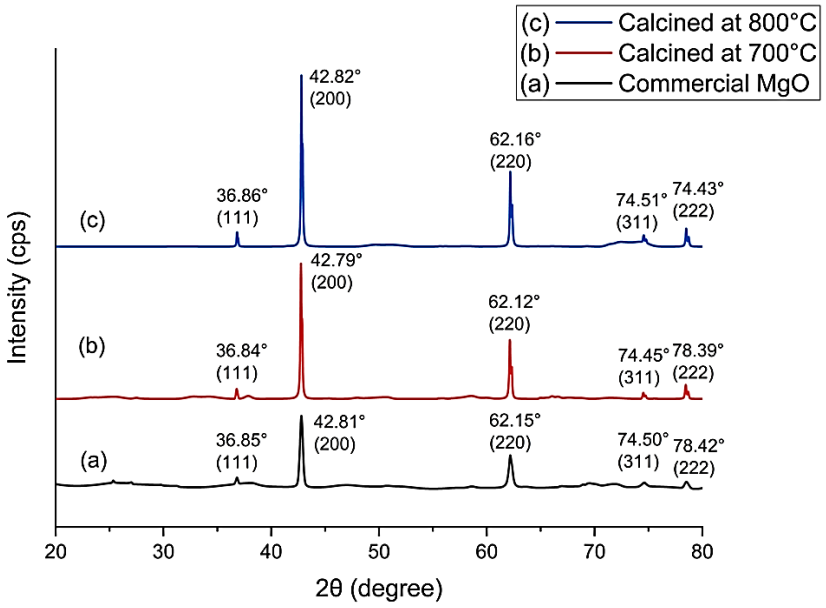

Figure 4 XRD diffractograms of commercial and synthesized MgO

Table 3 XRD data of commercial and synthesized MgO

Sample	2θ	d (angles)	d references (angles)	hkl
MgO-NPs calcined at 800 °C	36.86	2.437	2.438	111
	42.82	2.110	2.111	200
	62.16	1.492	1.493	220
	74.51	1.272	1.273	311
	78.43	1.218	1.219	222
MgO-NPs calcined at 700 °C	36.84	2.438	2.438	111
	42.79	2.111	2.111	200
	62.12	1.493	1.493	220
	74.45	1.273	1.273	311
	78.38	1.219	1.219	222
Commercial MgO	36.85	2.437	2.438	111
	42.81	2.110	2.111	200
	62.15	1.492	1.493	220
	74.50	1.273	1.273	311
	78.42	1.218	1.219	222

3.2.3 Scanning Electron Microscope (SEM)

SEM has been used to analyze the surface morphology, particle size, and distribution of the MgO-NPs. The dimensions of the particles were observed at 30,000X with energy at 10 keV and scales at 2 µm. Figure 5(a) shows the morphology of commercial MgO, where it can be seen that commercial MgO is highly agglomerated into larger clusters with some small particles in between. These particles exhibit an irregular, blocky, spherical shape with a rough, porous texture with sharp edges. Figure 5(b) represents the MgO precursor before calcination, where the particles are irregular with smaller aggregates. SEM images of MgO-NPs calcined at 700 °C, as shown in Figure 5(c), indicates the particles as irregular with different sizes having pores on their surfaces. While Figure 5(d) presents the calcination at 800 °C producing smoother, regular particles of various dimensions.

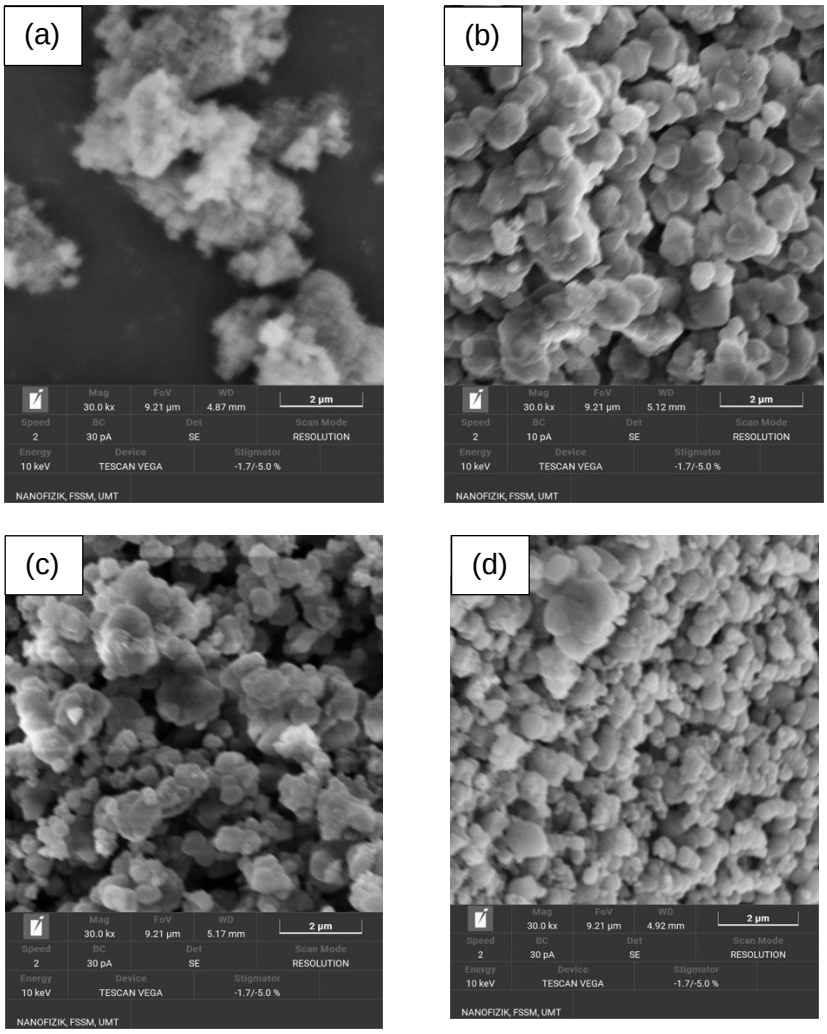

Figure 5 SEM images of commercial MgO (a), MgO precursor (b), MgO-NPs calcined at 700 °C (c), MgO-NPs calcined at 700 °C (d) at 30,000X magnification

SEM images significantly show changes in the morphology observed for MgO before and after calcination. In this regard, it is observed that the precursor MgO has irregular agglomerated particles with less porosity and a quite irregular surface promoting agglomeration. The particles after calcination at 700 °C are more dispersed with a smoother and regular surface, proving the elimination of impurities and water. At 800 °C, the particle size is a little greater than that at 700 °C, where the same case happens in the general morphology, resulting in a smoother surface with well-dispersed particles [7]. Table 4 presents the size range of MgO.

Table 4 Size ranges of commercial MgO and calcined MgO-NPs

Sample	Size range (nm)
Commercial MgO	138 – 233
MgO before calcine	209 – 469
MgO-NPs calcined at 700 °C	149 – 208
MgO-NPs calcined at 800 °C	170 - 298

3.2.4 UV-Vis Spectroscopy (UV-Vis)

UV-Vis analysis was used to observe the absorbance peak. Figure 6 represents the UV-Vis spectra of MgO-NPs calcined at 700 °C and 800 °C, showing absorption peaks at 348 nm and 346 nm, respectively. These are in the range between 270 nm and 374 nm as shown by previous works to confirm the presence of MgO-NPs [6,15]. The spectra appear similar, but the peak for the 800 °C sample is slightly shifted, indicating an increase in the band gap energy [2].

The band gap energy of MgO was calculated using Tauc plots and Eq. 1, 2, and 3 below.

$$(\alpha h\upsilon) = C(h\upsilon - Eg)n \quad (1)$$

where α is the absorption coefficient of the MgO at a certain value of wavelength λ, h is Planck's constant, C is the proportionality constant, υ is the frequency of light, Eg is the band gap energy and n=½ (for direct transition mode materials).

The absorption coefficient itself is calculated using Equation (2) :

$$\alpha = k \ln\left(\frac{Rmax\_Rmin}{R\_Rmin}\right) \quad (2)$$

where k is a constant and R_{max} and R_{min} represent the maximum and minimum reflectance values, respectively.

Combining these equations and rearranging simplifies the relationship to $(\alpha h\upsilon)^2$ proportional to (hυ - Eg), represented by Equation (3) :

$$(\alpha h\upsilon)^2 = C'(h\upsilon - Eg) \quad (3)$$

Figure 7 and Figure 8 show UV-Vis reflectance curves for commercial MgO and MgO-NPs calcined at 700 °C and 800 °C. Commercial MgO exhibits the highest reflectance, while MgO-NPs show lower reflectance, with further decreases at higher calcination temperatures [16].

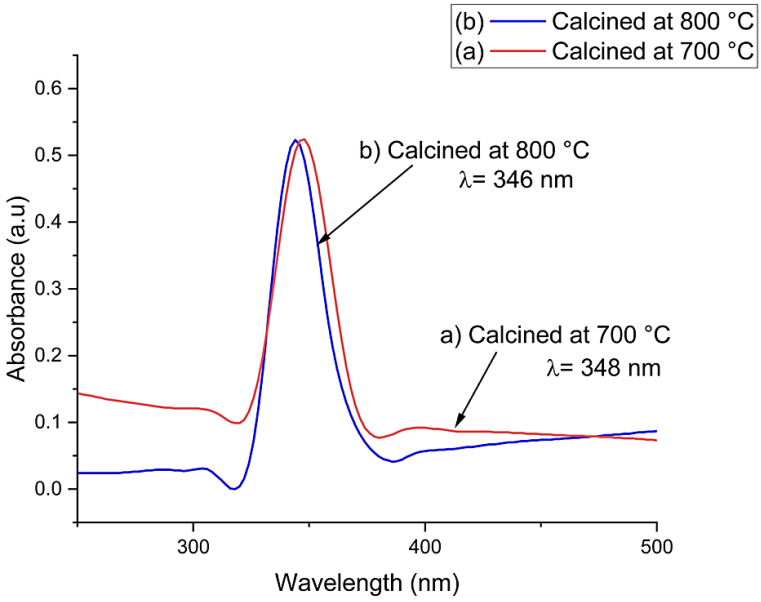

Figure 6 UV-Vis spectra of MgO-NPs calcined at 700 °C and 800 °C

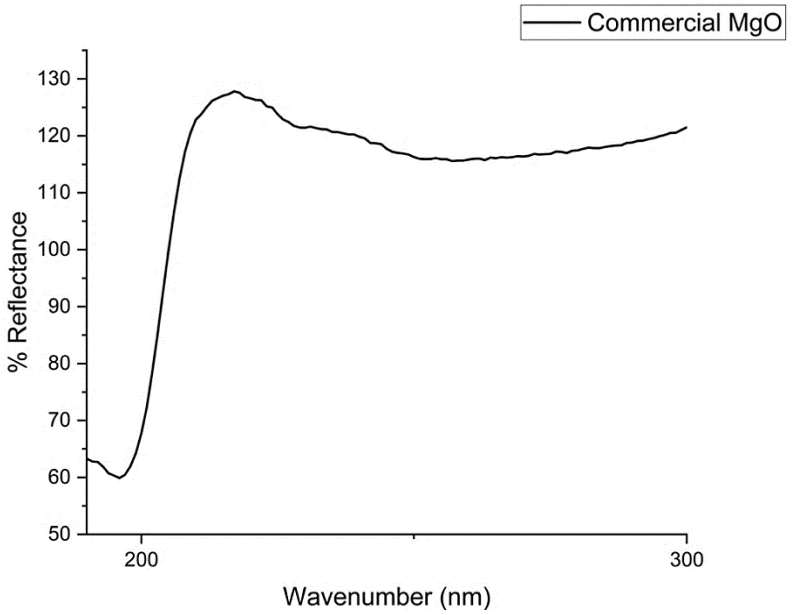

Figure 7 UV–Vis reflectance curves of the commercial MgO

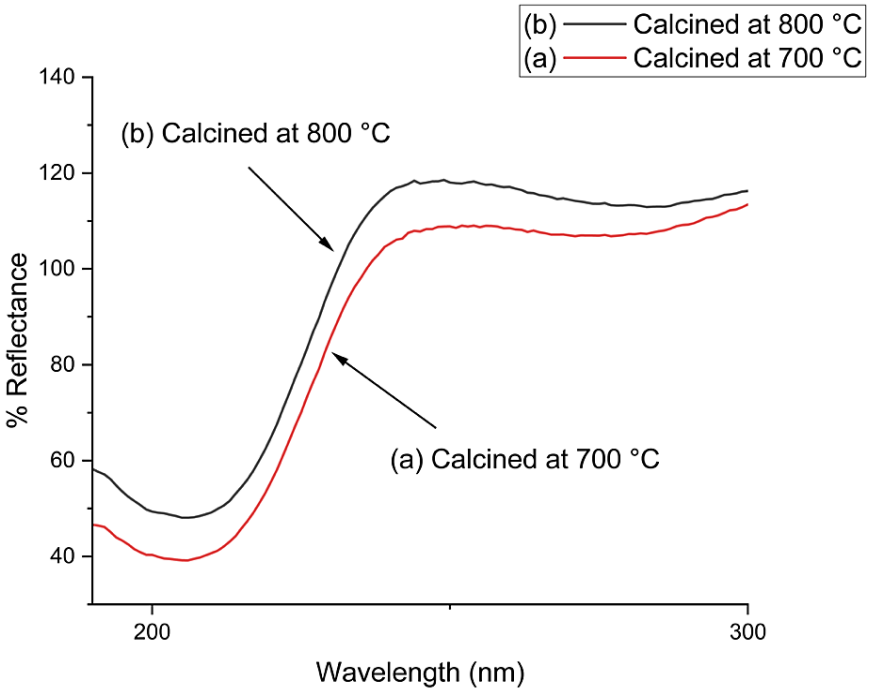

Figure 8 UV–Vis reflectance curves of MgO-NPs calcined at 700 °C (a) and 800 °C (b)

Tauc plots (Figure 9) depict commercial MgO with a band gap of 6.15 eV, while MgO-NPs calcined at 700 °C have a band gap of 5.58 eV, and those calcined at 800 °C have a band gap of 5.62 eV, illustrating an increase in crystallinity with higher calcination temperatures [17]. These results, supported by XRD and SEM analyses, demonstrate that higher calcination temperatures enhance the crystallinity of MgO-NPs, which is linked to the increase in band gap.

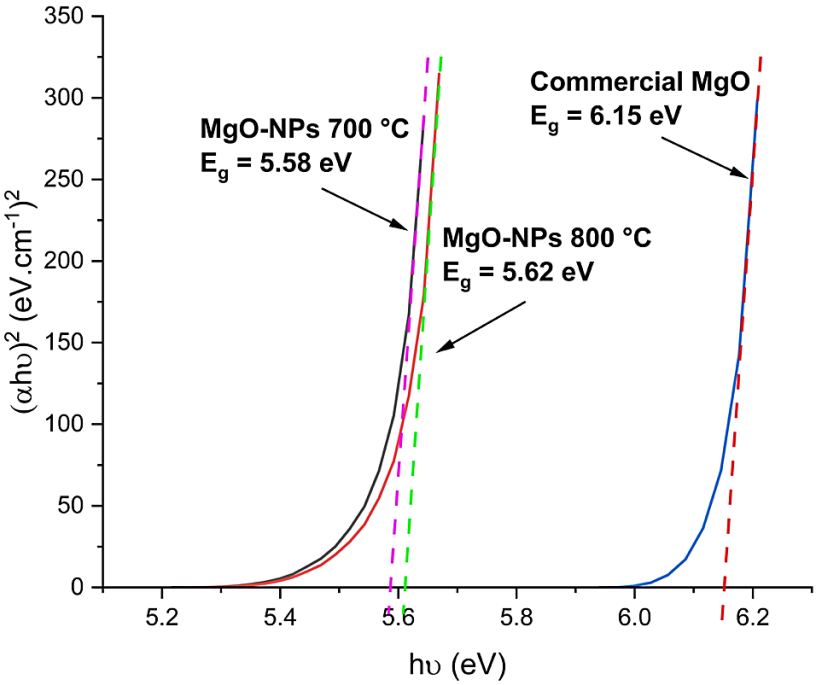

Figure 9 Tauc plots of commercial MgO and synthesized MgO-NPs

3.2.5 Accelerated Surface Area and Porosimetry (ASAP)

ASAP analysis was employed to evaluate the surface area and pore size distribution of MgO-NPs. Figure 10 displays the isotherm graphs for commercial MgO, MgO-NPs calcined at 700 °C, and MgO-NPs calcined at 800 °C, respectively, with the results summarized in Table 5.

The analysis showed a reduction in surface area with increasing calcination temperature, dropping from 21.05 m²/g at 700 °C to 3.66 m²/g at 800 °C. Concurrently, pore size increased from 67.50 Å at 700 °C to 128.56 Å at 800 °C, demonstrating that MgO calcined at 800 °C has larger, more porous particles.

These findings align with SEM images (Section 3.2.3), which depict particles calcined at 800 °C as larger and more porous compared to those calcined at 700 °C [18].

This trend reflects Type IV isotherms, indicative of mesoporous materials, with H3 hysteresis loops suggesting the presence of plate-like pores [19]. The reduction in surface area with increasing calcination temperature is attributed to sintering, where particles coalesce to form larger structures, thereby decreasing surface area [20]. This confirms MgO-NPs as mesoporous materials with distinct plate-like pores, as validated by the ASAP analysis.

Table 5 ASAP analysis of MgO

	BET Surface Area	Pore size	Isotherm type	Hysteresis type
Commercial MgO	21.9091 m^2/g	78.5863 Å	Type IV	H3
MgO calcined at 700 °C	21.0549 m^2/g	67.5032 Å	Type IV	H3
MgO calcined at 800 °C	3.6594 m^2/g	128.5620 Å	Type IV	H3

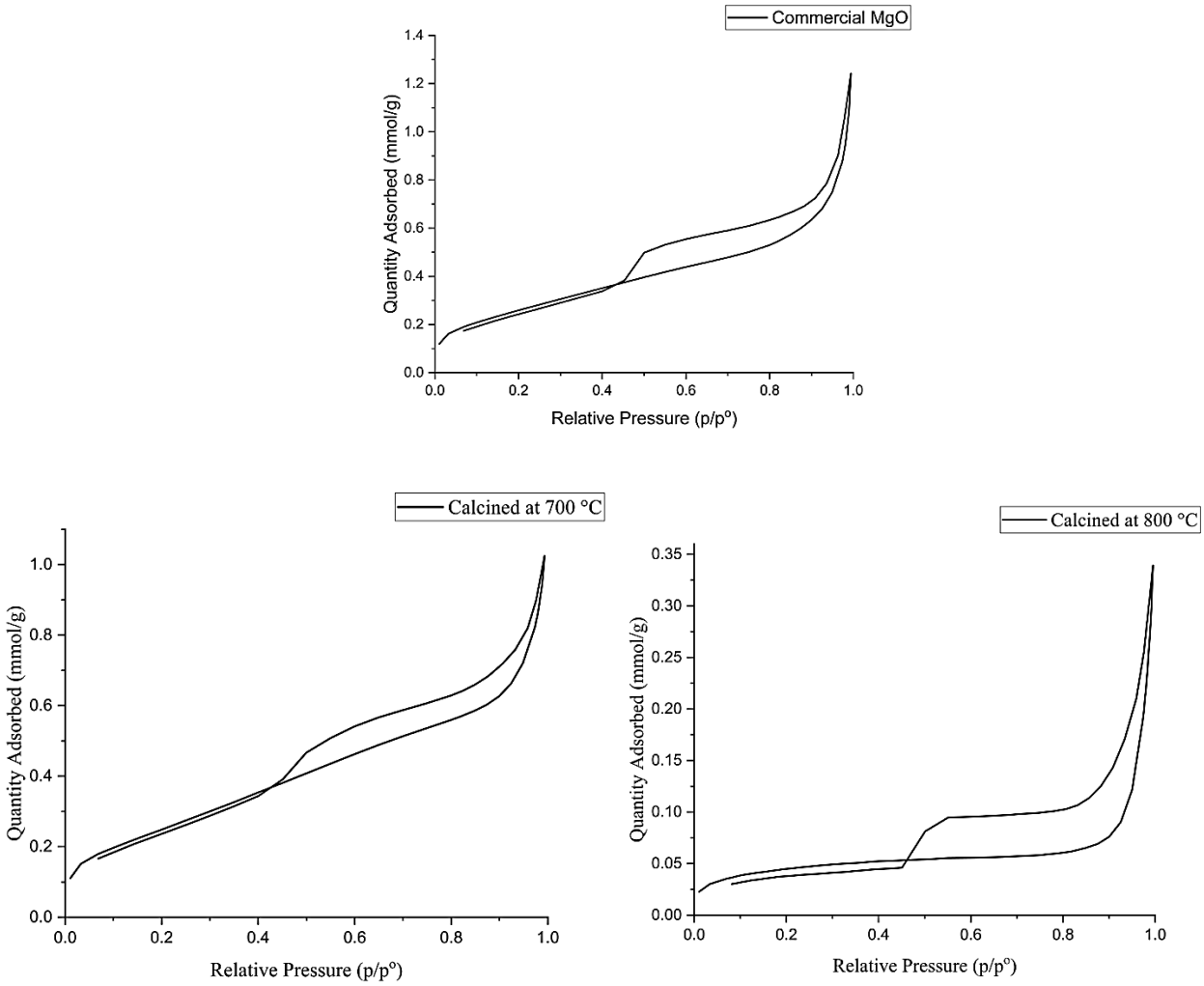

Figure 10 Isotherm graph of (a) commercial MgO, (b) MgO-NPs calcined at 700 °C and (c) MgO-NPs calcined at 800 °C

3.2 Antibacterial Activity

3.2.1 Magnesium Oxide Nanoparticles (MgO-NPs) against Gram Positive and Gram Negative Bacteria

The antibacterial properties of MgO-NPs synthesized via the green combustion method were evaluated against Gram-positive *Staphylococcus aureus* (*S. aureus*) and Gram-negative *Escherichia coli* (*E. coli*) using the well-diffusion method. This method is commonly employed to assess antimicrobial activity by testing the inhibitory effects of substances on microbial growth [9-10].

The antibacterial activity of commercial MgO and calcined MgO-NPs (at 700 °C and 800 °C) was tested at concentrations ranging from 25 mg/mL to 500 mg/mL. Deionized water and Gentamicin served as a negative control and positive control, respectively. Table 6 presents the zone of inhibition (ZOI) results, with MgO-NPs calcined at 800 °C showing significant antibacterial activity against *S. aureus*, particularly at higher concentrations, while other concentrations did not show any inhibition zone. The positive control exhibited a ZOI of 21 mm against *S. aureus* and 16 mm against *E. coli*, confirming bacterial susceptibility. In contrast, the negative control showed no inhibition, indicating normal bacterial growth.

The antibacterial efficacy increased with MgO-NPs concentration, with the highest activity observed for MgO-NPs calcined at 800 °C, suggesting that calcination temperature influences antibacterial effectiveness. Notably, *S. aureus* was more sensitive to MgO-NPs than *E. coli*, consistent with findings by [9-10,21-22] and other studies. Gram-negative bacteria show less sensitivity as they are known for having outer membrane known as liposaccharide (LPS) [6, 23].

Table 6 Antibacterial activity of MgO-NPs

	Zone of Inhibition (mm)			
	MgO-NPs calcined at 700 °C		MgO-NPs calcined at 800 °C	
Bacteria	*S. aureus*	*E. coli*	*S. aureus*	*E. coli*
Positive control	21	16	21	16
Negative control	-	-	-	-
MgO-NPs 25 mg/ml	-	-	-	-
MgO-NPs 50 mg/ml	-	-	-	-
MgO-NPs 100 mg/ml	-	-	-	-
MgO-NPs 125 mg/ml	-	-	-	-
MgO-NPs 250 mg/ml	-	-	-	-
MgO-NPs 500 mg/ml	-	-	3	-

4.0 CONCLUSION

Magnesium oxide nanoparticles (MgO-NPs) have been successfully synthesized via green combustion method using *Asystasia gangetica* plant extract. Phytochemical analysis identified bioactive compounds such as alkaloids, flavonoids, and phenols, which likely facilitated the reduction and stabilization of MgO. Thermogravimetric analysis indicated the optimal calcination temperatures for MgO-NPs synthesis were 700 °C and 800 °C. Characterization techniques including FTIR, XRD, SEM, UV-Vis, and ASAP confirmed the nanoparticles' crystalline structure, small particle size (149-298 nm), smooth morphology, and mesoporous nature. Antibacterial testing revealed significant activity against Gram-positive *Staphylococcus aureus* at higher concentrations of MgO-NPs calcined at 800 °C, while no notable effect was observed against Gram-negative *Escherichia coli*, suggesting a greater susceptibility of *S. aureus*. Overall, MgO-NPs synthesized via this method have proven to be a potential antimicrobial agent and can be further explored and exploited. In future studies, it is suggested to synthesize MgO-NPs with various plant extracts and explore other Gram-positive and Gram-negative bacteria to further investigate the potential of MgO-NPs as antibacterial agent.

Acknowledgment

The authors would like to acknowledge the Organization for The Prohibition of Chemical Weapons (OPCW) for providing the research grant (project Account No: L/ICA/ICB-111/21) @ (UMT/PPP/2–2/25 Jld. 9 (93), No. Vot: 53480) for financial support for this project, as well as the Faculty of Science and Marine Environment, Universiti Malaysia Terengganu (UMT).

References

[1] Ansari, A., Ali, A., Asif, M., & Shamsuzzaman, M. (2017). Microwave-assisted MgO NP catalyzed one-pot multicomponent synthesis of polysubstituted steroidal pyridines. *New Journal of Chemistry, 42*(1), 184–197. https://doi.org/10.1039/C7NJ03742B

[2] Ashok, K. S., Jarvin, M., Sharma, S., Umar, A., Inbanathan, S. S. R., & Nayak, A. K. (2021). Facile and green synthesis of MgO nanoparticles for the degradation of Victoria Blue dye under UV irradiation and their antibacterial activity. *ES Food and Agroforestry, 5*, 14–19. https://doi.org/10.30919/ESFAF519

[3] Baig, N., Kammakakam, I., Falath, W., & Kammakakam, I. (2021). Nanomaterials: A review of synthesis methods, properties, recent progress, and challenges. *Materials Advances, 2*(6), 1821–1871. https://doi.org/10.1039/D0MA00807A

[4] Saidi, N. S. M., Ying, K. J., Yusoff, H. M., & Badar, N. (2023). Synthesis and characterization of magnesium oxide nanoparticles by using banana peel (Musa Acuminata Cavendish) extract. *Malaysian Journal of Analytical Sciences, 27*(5), 1017–1034.

[5] Saidi, N. S. M., Badar, N., Yusoff, H. M., & Elong, K. (2024). Effect of Zn, Ti, and Sn dopants on the structural, morphological, and optical properties of MgO nanoparticles synthesized via green combustion using *Persicaria odorata* leaves extract. *Emergent Materials.* https://doi.org/10.1007/s42247-024-00871-2

[6] Farizan, A. F., Yusoff, H. M., Badar, N., Bhat, I. U. H., Anwar, S. J., Wai, C. P., Asari, A., Kasim, M. F., & Elong, K. (2022). Green synthesis of magnesium oxide nanoparticles using *Mariposa christia vespertilionis* leaves extract and its antimicrobial study toward *S. aureus* and *E. coli*. *Arabian Journal for Science and Engineering, 48*(6), 7373–7386. https://doi.org/10.1007/S13369-022-07282-7

[7] Yusoff, H. M., Rafit, F. A., Mohamad, F. I., Hassan, N., & Daud, A. I. (2017). The effects of calcination temperatures in the synthesis of nanocrystalline magnesium oxide via sol-gel technique. *Applied Mechanics and Materials, 865*, 36–42. https://doi.org/10.4028/WWW.SCIENTIFIC.NET/AMM.865.36

[8] Idris, N. A., Aziz, N. A. A., Yusoff, H. M., Badar, N., Elong, K., Yusoff, F., Wai, C. P., & Hassan, N. (2023). Electrochemical performance of zinc oxide nanoparticles prepared via green synthesis route using *Chromolaena odorata* leaves extract as potential anode material in sodium-ion battery. *Journal of Sustainability Science and Management, 18*(10), 126–137. http://doi.org/10.46754/jssm.2023.10.008

[9] Balouiri, M., Sadiki, M., & Ibnsouda, S. K. (2016). Methods for in vitro evaluating antimicrobial activity: A review. *Journal of Pharmaceutical Analysis, 6*(2), 71. https://doi.org/10.1016/J.JPHA.2015.11.005

[10] Rotti, R. B., Sunitha, D. V., Manjunath, R., Roy, A., Mayegowda, S. B., Gnanaprakash, A. P., Alghamdi, S., Almehmadi, M., Abdulaziz, O., Allahyani, M., Aljuaid, A., Alsaiari, A. A., Ashgar, S. S., Babalghith, A. O., Abd El-Lateef, A. E., & Khidir, E. B. (2023). Green synthesis of MgO nanoparticles and its antibacterial properties. *Frontiers in Chemistry, 11*. https://doi.org/10.3389/FCHEM.2023.1143614

[11] Mugabo, P., & Raji, I. A. (2013). Effects of aqueous leaf extract of *Asystasia gangetica* on the blood pressure and heart rate in male spontaneously hypertensive Wistar rats. *BMC Complementary and Alternative Medicine, 13*, 283. https://doi.org/10.1186/1472-6882-13-283

[12] Pradita, T., Shih, S. J., Aji, B. B., & Sudibyo. (2017). Synthesis of MgO powder from magnesium nitrate using spray pyrolysis. *AIP Conference Proceedings, 1823*. https://doi.org/10.1063/1.4978089

[13] Khdary, N. H., Seddiq, W. K., Alkurdi, M. E., Alyamani, E. J., ALangari, A. A., & Aly-amani, E. J. (2019). Enhance the antimicrobial activity of silver nanoparticles by manipulating a redox process and controlling the size of the particles. *Biomedical Journal of Scientific & Technical Research, 16*(4), 1–9. https://doi.org/10.26717/BJSTR.2019.15.002882

[14] Thill, A. (2016). Characterisation of imogolite by microscopic and spectroscopic methods. *Developments in Clay Science, 7*, 223–253. https://doi.org/10.1016/B978-0-08-100293-3.00010-8

[15] Mamatha, K. M., Srinivasa Murthy, V., Ravikumar, C. R., Murthy, H. C. A., Kumar, V. G. D., Kumar, A. N., & Jahagirdar, A. A. (2022). Facile green synthesis of molybdenum oxide nanoparticles using *Centella Asiatica* plant: Its photocatalytic and electrochemical lead sensor applications. *Sensors International, 3*, 100153. https://doi.org/10.1016/J.SINTL.2021.100153

[16] Zhang, L., Wu, P., Chen, H., Yuan, L., Yang, G., Xie, H., Liang, D., Xie, J., Deng, L., & Al, -. (2019). Effect of calcination temperature on visible near-infrared reflectance of aluminum-doped chromium. https://doi.org/10.1016/j.mssp.2019.104672

[17] Chan, Y. B., Selvanathan, V., Tey, L. H., Akhtaruzzaman, M., Anur, F. H., Djearamane, S., Watanabe, A., & Aminuzzaman, M. (2022). Effect of calcination temperature on structural, morphological, and optical properties of copper oxide nanostructures derived from *Garcinia mangostana* L. leaf extract. *Nanomaterials, 12*(20). https://doi.org/10.3390/NANO12203589

[18] Koroth, S. K., Saji, A., Chanda, A., & Vasundhara, M. (2022). Effects of calcination temperatures on structural, optical, and magnetic properties of MgO nanoflakes and its photocatalytic applications. *Optical Materials, 132*. https://doi.org/10.1016/J.OPTMAT.2022.112777

[19] Thommes, M., Kaneko, K., Neimark, A. V., Olivier, J. P., Rodriguez-Reinoso, F., Rouquerol, J., & Sing, K. S. W. (2015). Physisorption of gases, with special reference to the evaluation of surface area and pore size distribution (IUPAC Technical Report). *Pure and Applied Chemistry, 87*(9–10), 1051–1069. https://doi.org/10.1515/PAC-2014-1117

[20] Huang, L., Yang, Z., & Wang, S. (2020). Influence of calcination temperature on the structure and hydration of MgO. *Construction and Building Materials, 262*, 120776. https://doi.org/10.1016/J.CONBUILDMAT.2020.120776

[21] Kauffmann, A. C., & Castro, V. S. (2023). Phenolic compounds in bacterial inactivation: A perspective from Brazil. *Antibiotics, 12*(4). https://doi.org/10.3390/ANTIBIOTICS12040645

[22] Kuo, Y.-C., Lin, S.-P., Lin, C.-W., Tsai, Y.-C., Wu, T.-S., & Hsiao, I.-L. (2023). Enhanced antibacterial activity in cellulose acetate films with surface defect-rich MgO nanoparticles for sustainable active packaging applications. *ACS Applied Nano Materials, 6*(21), 19915–19925. https://doi.org/10.1021/ACSANM.3C03724

[23] Basir, O. H., Zaid, N. A., Mohd Fauzi, N. A., & Razak, A. H. (2020). Characterization of *Asystasia gangetica* and *Phyllanthus niruri* extracts: Total phenolic content, antioxidant and antibacterial activities. *Journal of Sustainable Nature Resources*. https://doi.org/10.30880/jsunr.2020.01.02.006